Surface Roughness Effects of Pd-loaded Magnetic Microspheres on Reduction Kinetics of Nitroaromatics

Seonghwi An [ID],[†] Shanmugam Manivannan [ID],[†,‡,*] Mayavan Viji [ID],[§] Min Suk Shim,[¶]
Byeong Hee Hwang,[¶] and Kyuwon Kim [ID][†,*]

[†]*Electrochemistry Laboratory for Sensors & Energy (ELSE), Department of Chemistry, Incheon 22012, Republic of Korea. *E-mail: kyuwon_kim@inu.ac.kr*
[‡]*Department of Chemistry, Institute of Science, Banaras Hindu University, Varanasi, Uttar Pradesh, 221005, India. *E-mail: smanivannan@bhu.ac.in*
[§]*College of Pharmacy and Medicinal Research Center (MRC), Chungbuk National University, Cheongju 28160, Republic of Korea*
[¶]*Division of Bioengineering, Incheon National University, Incheon 22012, Republic of Korea*

Metal nanoparticles decoration on magnetically active semiconductor materials is a common strategy to improve the colloidal stability, catalyst harvesting, and reuse. In this study, a surfactant-free solvothermal method followed by a heat treatment to prepare highly surface roughened α-Fe$_2$O$_3$ (Hematite)/Pd microspheres (MSPs) is reported. Amine-functionalized silicate sol-gel matrix is used as a stabilizing agent for the solvothermal synthesis of Prussian blue (PB) MSPs using HCl at 80 °C for 20 h. It is observed that modulating HCl concentration in a medium led to a high degree of improvement in surface roughness. Employing heat treatment at 350 °C for 6 h, PB MSPs are transformed into α-Fe$_2$O$_3$, Hematite phase. Fabricated Hematite/Pd MSPs have shown high catalytic reduction activity over p-nitrophenol. Reduction kinetics of nitroaromatics is monitored using UV-vis absorption spectroscopy and product formation is confirmed by ^{1}H and ^{13}C NMR analyses.

Keywords: Hematite, Palladium, p-nitrophenol, Prussian blue, Interfaces of catalysts

Introduction

For the industrial-scale synthesis of aromatic amines, such as amino phenol, it is more important to reduce the energy intake and chemical left-over in the chemical reactions are continuous tasks, as environmental apprehensions are progressively fetched into emphasis.[1–3] To fulfill an ever-growing demand for manufacturing dyes, pharmaceuticals, pesticides, explosives, fibers, production in a industrial scale for everyday requirement, production capacity of starting materials; aminophenol and other aromatic amines need to further increase.[4,5] Noble metal-based nanoparticles (NPs) have been extensively studied as high-performance catalysts in the fields ranging from chemical manufacture and energy harvesting to environmental protection.[6–9] Among the noble metal NPs, palladium (Pd)-based catalysts are very attractive because Pd is the central component of many catalysts[10–13] and electrocatalysts[8,14] applied in industrial processes and devices due to their distinctive catalytic properties. Usage of precious metal (Rh, Pt, Au, Ru, Ir, Os, Ag, and Pd) NPs in the catalysis has been restricted owing to its value, solemn aggregation problems, and inadequate abundance. To overcome these issues of precious metal NPs is to find appropriate solid-supports which can advance the applicability of precious metal NPs.

Nano- or micro-scaled metal oxide materials with permeable structures have attracted emergent consideration owing to its distinctive structural possessions and potential tenders in various fields, such as catalysis,[15–18] energy harvesting,[19,20] and chemical sensors.[21] In general, template-assisted and hydrothermal methodologies are common for preparing the transition metal oxides and they are often suffering from their limitations in handling hard (such as silica or carbon) and soft (such as long-chain polymers and surfactants) templates. Materials stability during an etching process of a hard template and identifying a suitable precursor as a soft template are of prime concern. Hence, identifying the alternative facile methodologies to fabricate the transition metal oxides with the desired morphologies are more preferred.

Herein, a general strategy for the surfactant-free solvothermal synthesis of Prussian blue (PB) microspheres (MSPs) with high surface roughness is reported, it was used as a precursor to obtaining Pd NPs decorated Hematite MSPs and catalytic activity of the resultant Hematite/Pd MSPs was verified toward reduction of Nitroaromatics to Aminoaromatics. At higher HCl concentration, the classical structure-directing agent, Polyvinylpyrrolidone (PVP) led to etched PB nanostructures (NSs) which is uncomplimentary hence, frequently grief from firmness and regularity

problems. On contrary, in this report, the silicate sol-gel matrix (SSG) offers highly surface roughened PB NSs which possess high uniformity and stability. Also, a large amount (for instance 3.75 g for 500 mL batch) of PVP is required for a batch and it is quite hard to make a homogenous reaction mixture due to its sticky nature and it is allergic to skin and respiratory system too. Considering an industrial-scale process, these obstacles need to be solved; the SSG matrix is a low-cost material and simple hydrolysis is enough to make it homogenous and offers mild reaction conditions. Hence, SSG is the suitable alternative as a structure-directing agent for PB NSs to the classical PVP. Quantitative kinetic analysis is imperative to understand the impact of the surface roughness on the catalytic activity of the nanocomposites. Model reaction of p-nitrophenol (PNP) with $NaBH_4$ to p-aminophenol (PAP) with $NaBH_4$ demonstrates an interesting surface roughness-dependent catalytic activity of the Hematite/Pd MSPs catalyst.

Experimental

Synthesis of PB MSPs and Cubes. In brief, 0.5 mL of 1 M silane precursor was introduced into 500 mL of 0.01 M HCl or 500 mL of 0.1 M HCl solution and stirred well for 1 h. During the stirring, silane precursor get hydrolyzed into a silicate sol-gel matrix. Subsequently, 1.65 g of $K_3[Fe(CN)_6]$ was introduced and stirred for an another 30 min to get the homogenous solution. The reaction vessel was well sealed using aluminum foil and kept in an electric oven at 80 °C for 20 h. Afterward, reaction vessel has been taken out and allowed to cool down by air. Obtained precipitate was cautiously centrifuged with deionized (DI) water and ethanol three times. Subsequently, precipitate was dried at 80 °C. To acquire the PB Cubes, 3.75 g of PVP and 1.10 g of $K_4[Fe(CN)_6]$ were added instead of silane precursor and $K_3[Fe(CN)_6]$, respectively, in the presence of 0.1 M HCl. PB MSPs prepared using 0.01 M and 0.1 M of HCl have been denoted as PB(smooth) MSPs and PB(rough) MSPs, respectively.

Synthesis of PB/PdCN MSPs. Purified 50 mg of PB(smooth) MSPs (or) PB(rough) MSPs was disseminated by sonication in 50 mL of DI water and stirred at 80 °C in a water jacket container which is sealed with an aluminum foil. Subsequently, 1.33 mM of Pd precursor (Na_2PdCl_4) was introduced dropwise into the reaction mixture and the heating was continued for an another 1 h under mild stirring. A dark-green precipidate was carefully purified by centrifugation with DI water and ethanol and dried. The attained product is referred as PB(smooth)/PdCN MSPs or PB(rough)/PdCN MSPs.

Conversion of PB MSPs into Hematite MSPs. Purified PB MSPs (or) PB/PdCN MSPs (nonmagnetic and blue) was kept in a ceramic boat and annealed at 350 °C, 6 h in a Muffle furnace to get Hematite MSPs or Hematite/ Pd MSPs.

Results and Discussion

Morphological Properties of PB and Hematite/Pd Composites. The structural and surface roughness of PB precursors, Hematite, and Hematite/Pd nanocomposites were investigated by the scanning electron microscopy (SEM) analysis, as shown in Figure 1, Supporting Information - Figures S1 and S2. One can see that the capping agent and slight change in an experimental parameter had a substantial consequence on the resultant morphology. In the presence of PVP as stabilizer; only PB Cubes were obtained. On contrary, PB MSPs were obtained in the presence of SSG. The 0.01 M HCl has brought the lower surface roughness, although dispersed MSPs were still a major morphology (Figure 1(b) and (b1)). With increasing concentration of HCl from 0.01 M to 0.1 M, MSPs had become highly surface roughened (Figure 1(c) and (c1)), and no dispersed Cubes were observed. From the Figure 1(a), it can be learned that PVP is responsible for the uniform shape and sized PB Cubes growth, further revealing its vital role in directing a cubic morphology. When a capping agent was switched from PVP to SSG; –NH and $-NH_2$ groups of the SSG will develop an adsorption layer over nucleated PB particles, stabilize them and thereby having the control over the growth. Thereby, large PB crystals growth and aggregation among the smaller particles have controlled by the SSG.[22,23]

We observed a preliminary nucleation speed of PB have principally sluggish hence the growth of the PB particles is slow. The concentration of Fe^{2+} plays vital role in nucleation degree which ensued from a two-step procedure: the slow severance of $[Fe(CN)_6]^{3-}$ ions into Fe^{3+} ions, followed by reduction of Fe^{3+} ions into Fe^{2+} ions in the presence of SSG. The release of Fe^{2+} will be resolute by a first step since weak severance of $[Fe(CN)_6]^{3-}$ ions, which fluctuates on the temperature and HCl concentration. In the
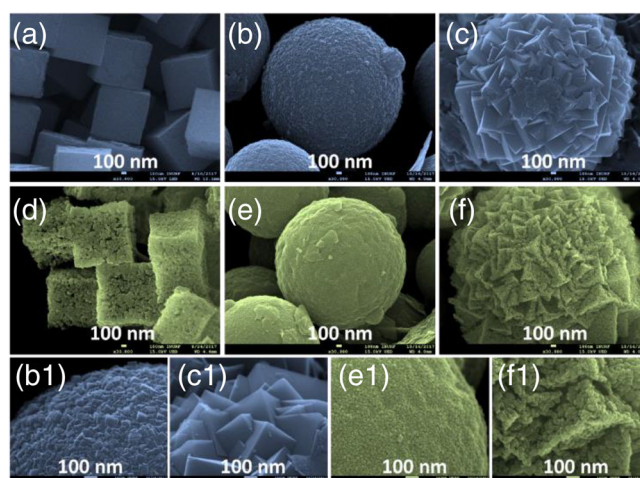

Figure 1. SEM images of (a) PB cubes, (b, b1) PB(smooth) MSPs, (c, c1) PB(rough) MSPs, (d) Hematite cubes, (e, e1) Hematite(smooth) MSPs, and (f, f1) Hematite(rough) MSPs.

presence of 0.01 M HCl, severance of $[Fe(CN)_6]^{3-}$ ions was sluggish, and the preliminary nuclei were scarce at beginning. The sluggish rate of nucleation was promising for consistent spherical morphology as predicted by the classical theory of crystal growth.[24,25] When HCl concentration is switched from 0.01 to 0.1 M, the nucleation rate got enhanced, consequently smaller cubical particles were attained. Owing to the inclination to diminish the entire surface energy, the smaller cubical particulates were accumulated in a methodical mode. Finally, even MSPs have grown through by unifying small cubical particles in the presence of SSG and this phenomenon led to a very high surface roughness.

Both PB Cubes and MSPs with typical size of 1 μm and unvarying size dispersal is noticed (Figure 1 and Supporting Information Figure S1), and Figure 1 (b) and (c) displays an instance of single MSP demonstrating variation in the surface roughness (higher magnification; Figure 1(b1) and (c1)) between PB MSPs prepared in the presence of two different concentrations of HCl. Due to the 6 h of annealing at 350 °C, PB Cubes and MSPs were transformed into Hematite Cubes and MSPs, owing to an oxidative thermal breakdown of the PB, and corresponding SEM images were concise in Figure 1(d)–(f) and Supporting Information Figure S1 along with their higher magnified images; Figure 1(e1) and (f1). When PB MSPs were treated with Pd precursor (Na_2PdCl_4), the color of a suspension switched blue to dark green. Uniformity in growth emergent on surface of PB MSPs (Supporting Information Figure S2(a) and (b)). High magnification SEM image (Supporting Information Figure S2(b1) and (c1)) had revealed that evolutions are PdCN gangs with 10–100 nm in size (particles grown on a surface). The SEM images had also revealed few more PdCN gangs, representing that PdCN would breed additional bigger musters and might reach maximum of 150 nm. Supporting Information Figure S2(c), (c1), (d), and (d1) is representing the SEM images after a heat treatment. Thermal breakdown brought porous Hematite MSPs and interestingly the morphology had been retained after a heat treatment. scaning electron microscopy-enenrgy dispersed x-ray elemental mapping (Supporting Information Figure S2(a2), (b2), (c2), and (d2)) of both PB/PdCN MSPs and Hematite/ Pd MSPs confirms the consistent dispersal of the Pd NPs over PB and Hematite MSPs. The x-ray difraction, thermogravimetric analysis, and x-ray photoelectron spectroscopy analyses were carried out and the discussion part is given in Supporting Information Figures S3 and S4.

Furthermore, the structural morphology of the Hematite(rough)/Pd MSPs were further confirmed by transmission electron miscroscopy (TEM) images (Figure 2). An enlarged TEM pictures (Figure 2(a)–(d)) are representative of astonishing surface roughness, signifying an admirable physical solidity of the composites. The magnified TEM picture (Figure 2(b)) of single MSP validate its rock-hard structure and porosity; besides, loaded Pd NPs is
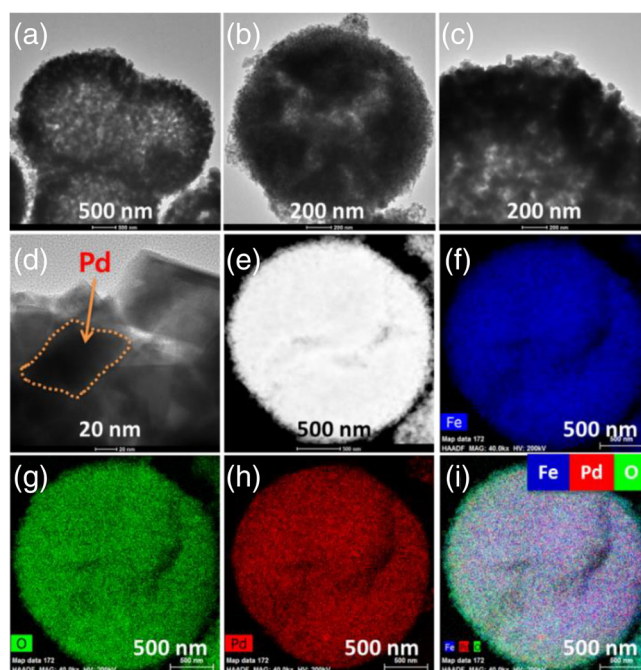

Figure 2. (a–d) TEM images, (e) STEM-HAADF, and (f–i) STEM-EDX elemental mapping analyses of Hematite(rough)/ Pd MSPs.

distinguishable from Hematite surface, due to its contrast difference; the former is seeming as dark and late is seeming as gray owing to difference in their electron densities (Figure 2(d)). Pd NPs were perceived lone at the outsides of the Hematite MSPs and remarkably, cavities awakened from the damage of crystallization water and exclusion of inorganic residues during a thermal decomposition was visible at the center (Figure 2(c)). Supporting Information - Figure S5 reveals the STEM-EDX elemental composition analysis of a Hematite(rough)/Pd MSPs, inductively coupled plasma-mass spectrometry analysis reveals the atomic contributions of Fe and Pd from the Hematite(smooth)/Pd MSPs, and Hematite(rough)/Pd MSPs were identified as 94.7%:5.3% and 96.1%:3.9%, respectively and suggesting that Pd NPs are efficaciously encumbered over Hematite. The resultant scanning transmission electron microscopy-high-angle annular dark-field imaging (STEM-HAADF) image (Figure 2(e)) is representing the crystalline characteristic of a catalyst and STEM-EDX (Figure 2(f)–(i)) of a catalyst is demonstrating that Hematite(rough)/Pd MSPs is composed of Fe, O, and Pd; among them Figure 2(h) is a concrete evidence for the effective confession of Pd NPs over Hematite and traces of Pd NPs on Hematite MSPs is uniform throughout the MSPs. Besides, an elemental mapping analysis is representative for catalyst is free from C and N elements aroused from –CN group signifying that PB MSPs were entirely converted into pure Hematite MSPs in annealing progression.

Catalytic Investigation. PNP is a serious intractable environmental pollutant frequently existing in effluent of chemical industries. On catalytic reduction, PNP will give a PAP and it is 500 times less toxic than a PNP and suitable for many submissions that comprise pain-relieving, corrosion inhibitors, febrifuge drugs, vivid designers, and so on.[26,27] The reaction of PNP to PAP with NaBH$_4$ as a typical system for testing the catalytic performance of Hematite/Pd MSPs Nanocomposites. The progress of the reduction was observed by UV-vis spectrophotometer. Comparison of standard electrode potentials of PAP and NaBH$_4$ reveals that the values are greater than zero ($\Delta E^0 = E^0_{(PNP/PAP)} - E^0_{(H3BO3/BH4)} = -0.76 - (-1.33) = 0.67$ V)[28] hence, reduction of PAP by NaBH$_4$ is thermodynamically feasible; however, it is kinetically restricted and requires a catalyst to proceed. PNP exhibit a distinct spectral peak at 317 nm, on adding NaBH$_4$, PNP is changed to p-nitrophenolate ion under basic condition, and do exhibit a peak maximum at 400 nm (Figure 3(a)). Figure 3(b) and (c) shows a UV-vis spectra with time for Hematite(smooth)/Pd MSPs and Hematite(rough)/Pd MSPs catalysts. Noble metal NPs alone and supported onto the suitable solid-supports are the most appropriate candidates for catalyzing a PNP by NaBH$_4$. To verify the impact of our solid support, controlled experiments were first performed. As PB Cubes or PB MSPs or Hematite MSPs were added into a reaction mixture, peak at 400 nm has gradually increased to some extent for the PB Cubes and PB MSPs whereas a peak remained unaltered for the Hematite MSPs concerning response, as presented in Supporting Information Figure S6. Furthermore, a peak at 300 nm conforming to a reaction produce PAP is absent. This specifies that both PB and Hematite alone do not have catalytic activity toward PNP. Besides, the commercial Pt/C displayed poor efficacy ($k = 0.321 \times 10^{-2}$ s^{-1}) and it is representative of sluggish electron transfer kinetics at Pt/C (Supporting Information Figure S8(a) and (b)). Whereas the commercial Pd/C displayed the better efficacy ($k = 3.264 \times 10^{-2}$ s^{-1}) (Supporting Information Figure S8(c) and (d)). On contrary, as the catalyst loaded Pd NPs, the strength of the absorption peak at 400 nm progressively diminished with growing reaction time for Hematite(smooth)/Pd MSPs (Figure 3(b)) and Hematite(rough)/Pd MSPs (Figure 3(c)). Simultaneously, a new absorption peak confirming the formation of PAP had seemed at 300 nm and progressively improved. Also, after the addition of a catalyst, vanishing and eventual whitening of yellow-green of p-nitrophenolate ions in a reaction was observed, enlightening the reduction of PNP to form PAP. Upon completion, a peak owed to a nitro composite is completely quenched, representing that the reduction of PNP had progressed positively. Besides, noticed isosbestic point (Figure 3(b)) other than PAP. Also, to acquire rate constant, an absorption intensity of the PNP at time t is designated as "C_t" and the early absorption intensity of PNP at $t = 0$ is allocated as "C_0." From the comparative intensity owing to absorbance extinction "C_t/C_0" values were
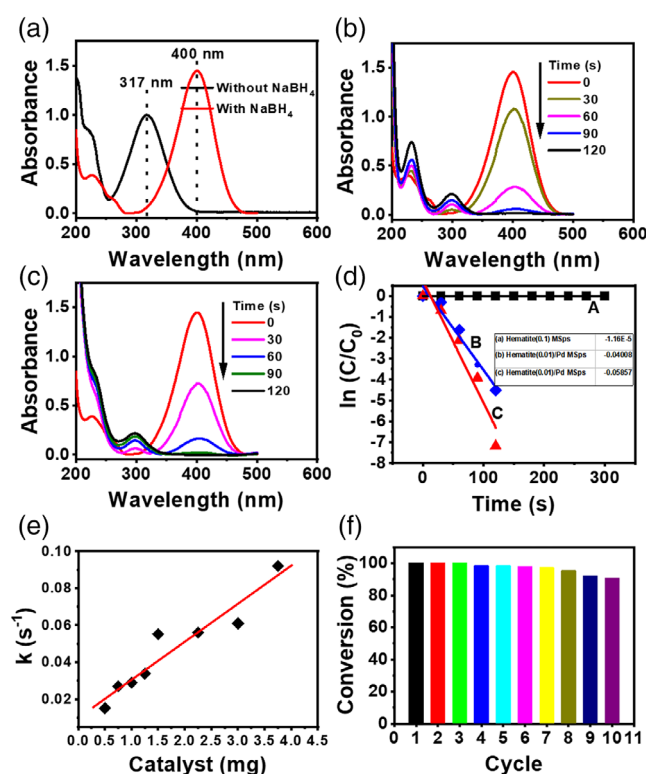

Figure 3. (a) UV-vis spectra of PNP before and after addition of NaBH$_4$. (b, c) Reduction of PNP in aqueous solution recorded every 30 s using (b) Hematite(smooth)/Pd MSPs and (c) Hematite (rough)/Pd MSPs. (d) Relationship between ln(C_t/C_0) and reaction time (*t*); (A) Hematite(rough) MSPs, (B) Hematite(smooth)/Pd MSPs, and (C) Hematite(rough)/Pd MSPs. (e) The relationship between the pseudo-first-order rate constant and the catalyst amount; (f) The reusability of Hematite(rough)/Pd MSPs for the reduction of PNP with NaBH$_4$ products obviously Hematite (rough)/Pd MSPs displays better performance than the Hematite(smooth)/Pd MSPs. Because, Hematite MSPs alone is inactive for PNP reduction (Supporting Information Figure S6), so the active part of Hematite/Pd Nanocomposites is principally aroused from Pd NPs. The catalyst's surface morphology, more the roughened surface seems more efficient in supporting the Pd NPs for effective catalysis (Supporting Information Figure S2 (a) and (a2)). On contrary, at Hematite(rough)/Pd MSPs, Pd NPs were less aggregated, smaller in size, and had uniformly distributed throughout the roughened surface hence exhibiting a higher active surface area (Supporting Information Figure S2(d) and (d2)). Rate constants "*k*" of Hematite/Pd Nanocomposites is relatively higher than the previously reported substrate-supported NPs, as given in Table 1. Better performance of the Hematite(rough)/Pd MSPs could be attributed to a high surface roughened spherical Hematite with the well-distributed smaller-sized Pd NPs, permitting an operative interaction among the PNP and Pd NPs.

consequential and plotted against time (Figure 3(d)) for the Hematite(rough) MSPs, Hematite(smooth)/Pd MSPs, and Hematite(rough)/Pd MSPs catalysts. A linear association among ln(C_t/C_0) and time is representative of the catalytic reaction that had succeeded through a first-order response

Table 1. Comparison of catalytic activity of present hematite(rough)/Pd MSPs with relevant reported results.

Catalysts	$C_{\text{(p-nitrophenol)}}$ (mM)[a]	C_{pd} (mM)[b]	Catalyst (mol%)	C_{NaBH4} (mM)[c]	k_{app} (10^{-2} s^{-1})[d]	References[e]
Hematite(rough)/Pd MSPs	0.1	1.33	13.3	0.02	5.850	Here
Hematite(smooth)/Pd MSPs	0.1	1.33	13.3	0.02	4.007	Here
Pt/C (20% Alfa Aesar)	0.1	-	-	0.02	0.321	Here
Pd/C (20% Alfa Aesar)	0.1	-	-	0.02	3.264	Here
Pd60 Nanospheres	0.085	0.079	0.929	0.015	2.700	29
M−Au−K10 NDs	0.002	0.025	12.5	12.5	2.98	30
12%Pd@Fe$_2$O$_3$	0.1	0.015	0.15	-	4.90	31
rGS/Fe$_2$O$_3$-Pd/NCS	2.39	-	-	0.440	9.78	32
SPB-PS/Pd	0.1	0.000366	0.366	10.0	0.441	33
Al$_2$O$_3$/Pd	0.1	0.00848	8.48	0.000132	0.920	34

[a] C: concentration.

[b] C_{pd}: concentration of Palladium.

[c] C_{NaBH4}: concentration of sodium borohydride.

[d] k_{app}: apparent rate constant.

[e] Data were given or calculated in the respective papers; some data were not obtained.

kinetics. The measured kinetic rate constant (k) and time spent are 1.1153×10^{-5}, 4.4008×10^{-2}, and 5.8570×10^{-2} s^{-1}, and 0 (no reaction), 120, and 120 s, respectively. As can be seen from the rate constants, Obviously, hematite(rough)/Pd MSPs is having higher catalytic activity than the hematite(smooth)/Pd MSPs.

Figure 3(e) reviews the optimizing the catalyst dose; the plot tells that the rate of reaction is improved though growing a catalyst dose and it is typical for pseudo-first-order reactions. A catalyst dose of 1.5 mg is optimized and used for the study. To investigate reusability, later finishing the reaction, catalyst was magnetically separated and washed and reused. As shown in Figure 3(f), catalysts can be effectively reprocessed and reused for at least 10 cycles and extends possibility for industrial usage. Catalyst harvesting and reusability, possible mechanism for PNP reduction, and device fabrication for purification of PNP contaminated water are summarized in Supporting Information - Figures S9–S11.

Laboratory Scale Reduction of Nitroaromatics. In general, the catalytic reduction reaction of nitroaromatics into aminoaromatics will be carried out in the presence of unfavorable chemicals such as strong acids and metals like lead (Pb) and tin (Sn). In an industrial-scale process, their usage is strictly limited due to their impact on environmental safety. Noble metals loaded on an environment-friendly solid-support material are ideal candidates for such scale-up processes and such catalysts are receiving much attention in recent years due to their outstanding catalytic activities. Magnetically separable, environment-friendly, high resistance to corrosion and low-cost solid-support such as Hematite loaded with Pd NPs are more expedient for catalytic reduction reaction with the assistance of NaBH$_4$. Discriminative reduction reaction of nitro functional-groups in the presence of other reducible

functional groups is a tedious task for manufacturing functionalized anilines as a precursor for obtaining a variety of value-added fine chemicals. In this regard, nitro group reductions were accomplished in the presence of amine and hydroxyl groups. Supporting Information - Table S1 shows reduction of different nitro compounds using a Hematite(rough)/Pd MSPs catalyst. Product conversion was analyzed and confirmed by recording the ^{1}H NMR and ^{13}C NMR spectra and are shown in Supporting Information Figures S12–S21.

Conclusion

An environmentally benign catalyst and facile method for a catalytic reduction of nitroaromatics to arylamines has been demonstrated. Catalytic activity toward PNP reduction has been found to depend on a solid substrate's high surface roughness and uniform distribution of the loaded Pd NPs on it. And this assorted catalyst has demonstrated to be extremely effective, easily separable, and environmental in a catalytic reduction reaction under aqueous conditions. Significantly enhanced catalytic activity (120 s; $k = 5.8570 \times 10^{-2}$ s^{-1}) of Hematite(rough)/Pd MSPs was compared with a less surface roughened Hematite(smooth)/Pd MSPs (120 s; $k = 4.4008 \times 10^{-2}$ s^{-1}), which can be attributed to the electron transmission from BH$_4^-$ to Pd NPs, electron augmentation on the Pd NPs surface had facilitated the electron transmission from BH$_4^-$ to 4-nitrophenolate which is adsorbed neighboring surface roughened Hematite. Hematite(rough)/Pd MSPs exhibited excellent catalytic firmness and competence for cleansing PNP contaminated water. Given ease in product parting and catalyst harvesting and trivial reaction environments, as-prepared catalyst could find industrial applications and degradation of environment polluting

organic compounds. Furthermore, this simple, low-toxic, and low-cost method of making highly surface roughened Hematite MSPs with an innate three-dimensional structure and improved uniformity can be anticipated to be used as basic catalysts particularly making other "magnetic nanocatalysts" offering an opening to adventure new the catalytic constituents for the practical application in the more interesting reactions.

Supporting Information. Additional supporting information may be found online in the Supporting Information section at the end of the article.

References

1. J. Lv, Q. Zhang, M. Cai, Y. Han, S. Luo, *Chem. Asian J.* **2018**, *13*, 740.
2. B. Paul, S. Shee, D. Panja, K. Chakrabarti, S. Kundu, *ACS Catal.* **2018**, *8*, 2890.
3. K. Kang, H. Jang, *Bull. Korean Chem. Soc.* **2018**, *39*, 1231.
4. E. Menumerov, R. A. Hughes, S. D. Golze, R. D. Neal, T. B. Demille, J. C. Campanaro, K. C. Kotesky, S. Rouvimov, S. Neretina, *ACS Catal.* **2018**, *8*, 8879.
5. X. Yang, Y. Li, P. Zhang, R. Zhou, H. Peng, D. Liu, J. Gui, *ACS Appl. Mater. Interfaces* **2018**, *10*, 23154.
6. W. Liu, Y. Yu, J. Du, C. Jing, *J. Hazard. Mater.* **2019**, *366*, 338–345.
7. S. Qin, L. Y. Ma, X. Sun, X. Mao, L. Xu, *J. Hazard. Mater.* **2019**, *366*, 529–537. https://www.sciencedirect.com/science/article/abs/pii/S0304389418311737.
8. M. Song, Y. Wu, C. Xu, X. Wang, Y. Su, *J. Hazard. Mater.* **2019**, *368*, 530.
9. S. Manivannan, D.-K. Kang, K. Kim, *Bull. Korean Chem. Soc.* **2019**, *40*, 297.
10. T. Haynes, O. Ersen, V. Dubois, D. Desmecht, K. Nakagawa, S. Hermans, *Appl. Catal. B* **2019**, *241*, 196.
11. M. Nasrollahzadeh, Z. Issaabadi, R. Safari, *Sep. Purif. Technol.* **2019**, *209*, 136.
12. C. A. Teles, P. M. de Souza, R. C. Rabelo-Neto, M. B. Griffin, C. Mukarakate, K. A. Orton, D. E. Resasco, F. B. Noronha, *Appl. Catal. B* **2018**, *238*, 38.
13. R. Zhiani, M. Khoobi, S. M. Sadeghzadeh, *Microporous Mesoporous Mater.* **2019**, *275*, 76.
14. H. Liu, M. Wang, X. Zhang, J. Ma, G. Lu, *Appl. Catal. B* **2018**, *237*, 563.
15. S. Zhou, M. Johnson, J. G. C. Veinot, *Chem. Commun.* **2010**, *46*, 2411.
16. A. Bak, S. K. Choi, H. Park, *Bull. Korean Chem. Soc.* **2015**, *36*, 1487.
17. M. M. Rahman, X. B. Li, N. S. Lopa, J. J. Lee, *Bull. Korean Chem. Soc.* **2014**, *35*, 2072.
18. Z. Zhang, Q. Wu, X. Bu, Z. Hang, Z. Wang, Q. Wang, Y. Ma, *Bull. Korean Chem. Soc.* **2018**, *39*, 71.
19. Q. Qu, G. L. Pan, Y. T. Lin, C. W. Xu, *Int. J. Hydrogen Energy* **2018**, *43*, 14252.
20. N. Yang, S. Ni, Y. Sun, Y. Zhu, *J. Mol. Catal.* **2018**, *452*, 28.
21. A. Singh, A. Sharma, M. Tomar, V. Gupta, *Surf. Coat. Technol.* **2018**, *343*, 49.
22. X. Shen, S. Wu, Y. Liu, K. Wang, Z. Xu, W. Liu, *J. Colloid Interface Sci.* **2009**, *329*, 188.
23. H. J. Maeng, D. H. Kim, N. W. Kim, H. Ruh, D. K. Lee, H. Yu, *Curr. Appl. Phys.* **2018**, *18*, S21.
24. S. Auer, D. Frenkel, *Nature* **2001**, *409*, 1020.
25. T. Uemura, Y. Hoshino, S. Kitagawa, K. Yoshida, S. Isoda, *Chem. Mater.* **2006**, *18*, 992.
26. Z. Jiang, D. Jiang, A. M. Showkot Hossain, K. Qian, J. Xie, *Phys. Chem. Chem. Phys.* **2015**, *17*, 2550.
27. S. Manivannan, M.-S. Kim, T. Yim, K. Kim, *ChemistrySelect* **2019**, *4*, 5185.
28. W. Ye, J. Yu, Y. Zhou, D. Gao, D. Wang, C. Wang, D. Xue, *Appl. Catal. B* **2016**, *181*, 371.
29. R. Bhandari, M. R. Knecht, *ACS Catal.* **2011**, *1*, 89.
30. P. Viswanathan, R. Ramaraj, *J. Chem. Sci.* **2018**, *130*, 1–10. https://www.ias.ac.in/public/Volumes/jcsc/130/01/0004.pdf.
31. Z. Jiang, D. Jiang, W. Wei, Z. Yan, J. Xie, *J. Mater. Chem. A* **2015**, *3*, 23607.
32. T. Yao, J. Zhang, Q. Zuo, H. Wang, J. Wu, X. Zhang, T. Cui, *J. Colloid Interface Sci.* **2016**, *468*, 62.
33. Y. Mei, Y. Lu, F. Polzer, M. Ballauff, M. Drechsler, *Chem. Mater.* **2007**, *19*, 1062.
34. S. Arora, P. Kapoor, M. L. Singla, *React. Kinet. Mech. Catal.* **2010**, *99*, 157.